

Cite this: *Nanoscale*, 2024, **16**, 1633

## Protein-guided biomimetic nanomaterials: a versatile theranostic nanoplatform for biomedical applications

Da-Gui Zhang,<sup>†a</sup> Yu-Jing Pan,<sup>†a</sup> Biao-Qi Chen,<sup>ID \*a</sup> Xiao-Chang Lu,<sup>a</sup> Qin-Xi Xu,<sup>a</sup> Pei Wang,<sup>b</sup> Ranjith Kumar Kankala,<sup>ID a</sup> Ni-Na Jiang,<sup>ID a</sup> Shi-Bin Wang<sup>ID a</sup> and Ai-Zheng Chen<sup>ID \*a</sup>

Over the years, bioinspired mineralization-based approaches have been applied to synthesize multifunctional organic–inorganic nanocomposites. These nanocomposites can address the growing demands of modern biomedical applications. Proteins, serving as vital biological templates, play a pivotal role in the nucleation and growth processes of various organic–inorganic nanocomposites. Protein-mineralized nanomaterials (PMNMs) have attracted significant interest from researchers due to their facile and convenient preparation, strong physiological activity, stability, impressive biocompatibility, and biodegradability. Nevertheless, few comprehensive reviews have expounded on the progress of these nanomaterials in biomedicine. This article systematically reviews the principles and strategies for constructing nanomaterials using protein-directed biomineralization and biomimetic mineralization techniques. Subsequently, we focus on their recent applications in the biomedical field, encompassing areas such as bioimaging, as well as anti-tumor, anti-bacterial, and anti-inflammatory therapies. Furthermore, we discuss the challenges encountered in practical applications of these materials and explore their potential in future applications. This review aspired to catalyze the continued development of these bioinspired nanomaterials in drug development and clinical diagnosis, ultimately contributing to the fields of precision medicine and translational medicine.

Received 30th October 2023,  
Accepted 16th December 2023

DOI: 10.1039/d3nr05495k

rsc.li/nanoscale

### 1. Introduction

Biomineralization is a common natural phenomenon involving organisms guiding and regulating the formation of inorganic minerals.<sup>1,2</sup> Within biomineralization, organic matrices, including organic molecules, polypeptides, proteins, and nucleic acids, act as nucleation sites for inorganic minerals, influencing crystal growth and assembly in biological environments,<sup>3–5</sup> and yielding ordered organic–inorganic composites with multi-stage structures. Several examples of these biomineral tissues include shells, teeth, bones, and biological shells. These biomineral tissues have crucial functions such as protection, support, movement, and feeding.<sup>6</sup> Moreover, bio-

minerals regulated by organisms often exhibit superior physicochemical properties compared to synthetic materials. For instance, natural shells, composed of 95% aragonite and 5% organic matter, possess strength and toughness of approximately 3000 times greater than synthetic calcium carbonate (CaCO<sub>3</sub>).<sup>7</sup> Therefore, under the guidance of living organisms, the amalgamation of inorganic minerals and organic matrices can yield materials with outstanding performance. Inspired by the natural biomineralization process, researchers have introduced biomimetic mineralization, a strategy to prepare biomineral-like organic–inorganic composites *in vitro* by mimicking the process of mineral growth in living organisms.<sup>8,9</sup> Importantly, organic matrices can reduce the energy barrier for crystal nucleation and promote the heterogeneous nucleation of inorganic minerals.<sup>10</sup> Therefore, the crystallization kinetics of inorganic substances may be modulated through the organic matrices, achieving the controlled deposition of inorganic minerals. With the intensive study of biomimetic mineralization technology, materials resembling shells, bones, and teeth have been successfully synthesized, holding their promise for significant roles in biomedicine.<sup>11–13</sup> By employing the biomimetic mineralization strategy and rational

<sup>a</sup>Fujian Provincial Key Laboratory of Biochemical Technology & Institute of Biomaterials and Tissue Engineering, College of Chemical Engineering, Huaqiao University, Xiamen 361021, China. E-mail: biaoqi.chen@hqu.edu.cn, azchen@hqu.edu.cn

<sup>b</sup>Jiangxi Provincial Key Laboratory of Oral Biomedicine, Jiangxi Province Clinical Research Center for Oral Diseases, School of Stomatology, Jiangxi Medical College, Nanchang University, Nanchang 330006, China

<sup>†</sup>These authors contributed equally to this work.

design, highly ordered organic–inorganic composites with controllable structures, good biocompatibility, and distinct performance can be fabricated, facilitating structural bionics.

In recent years, nanotechnology has witnessed substantial progress in material science and biomedicine, leading to the development of numerous organic–inorganic nanomaterials with exceptional properties for various biomedical applications, including drug delivery,<sup>14,15</sup> bioimaging,<sup>16</sup> and cancer therapy,<sup>17–19</sup> among others. These biomimetic materials exhibit excellent properties and biological functions. For example, Wang *et al.* utilized the biomimetic mineralization strategy to construct a calcium phosphate (CaP) mineral protective shell for a Japanese encephalitis vaccine, forming a core–shell nanosized vaccine particle (B-JEV).<sup>20</sup> The CaP shell effectively prevented the exchange of hydrogen bonds between the vaccine and the aqueous solution and realized the stable storage of the vaccine at room temperature without compromising its biological characteristics. During the process of inorganic mineral formation, organic matrices play a crucial role in the nucleation, growth, and assembly of inorganic minerals. Among various organic matrices, proteins are widely explored in biomineralization research due to their excellent mineralization capacity and low immunogenicity. They selectively bind to crystal surfaces, controlling crystal morphology, and can act as templates for crystal nucleation, inducing specific crystal orientation or growth.<sup>21–23</sup> Moreover, amino acids, the constituents of proteins, typically possess multiple functional groups, such as amino, carboxyl, hydroxyl, and thiol, facilitating the adsorption of inorganic metal ions and the subsequent nucleation and growth of inorganic substances on proteins. The resulting nanomaterials can be easily regulated by controlling parameters such as pH, temperature, and ionic strength. Considerably, nanomaterials prepared by protein-directed biomineralization and biomimetic mineralization strategies have the following advantages. (i) Mild and green preparation conditions: the synthesis of biomimetic nanomaterials can usually be carried out in the aqueous phase and at room temperature,

ensuring the safety of operation, effectively reducing energy loss, and greatly reducing the possibility of environmental pollution. (ii) Good physiological activity: with simple synthesis conditions and a mild preparation process (typically at room temperature), the physiological activity of proteins can be well preserved. (iii) Good physiological stability: biomimetic nanomaterials can be synthesized and modified under near-physiological conditions, ensuring their physiological stability as the synthetic environment is very close to the *in vivo* environment. (iv) Good biocompatibility and biodegradability: the main components of nanomaterials, such as CaP and CaCO<sub>3</sub>, can be considered endogenous substances, which do not produce notable biological toxicity.<sup>24,25</sup> Moreover, these materials are easily metabolized and excreted by the body, with the degraded products potentially serving as nutritional elements. These unique characteristics have attracted significant attention from researchers utilizing proteins as biological templates to prepare biomineralized nanomaterials.

Several reviews have discussed the utilization of organisms (*e.g.*, viruses, bacteria, and cells) and biomineralization technology to fabricate hybrid organic–inorganic materials and demonstrated their potential for diverse applications, such as cell protection, vaccine development, and cancer therapy. Nonetheless, there remains a dearth of systematic reviews consolidating protein-mineralized nanomaterials (PMNMs) and their applications in the biomedical field. Therefore, a timely review, and a systematic summary of the related work, would be of great significance for the continuous development of hybrid organic–inorganic nanomaterials. This review aims to comprehensively outline the general construction principles and strategies employed in preparing PMNMs. Furthermore, it systematically examines the application of these materials in biomedical domains, such as bioimaging, as well as anti-tumor, anti-bacterial, and anti-inflammatory therapies (Scheme 1). Furthermore, the review explores the potential challenges associated with these nanomaterials in practical applications, providing insights into their future utilization. Importantly, the



**Biao-Qi Chen**

*Biao-Qi Chen received his Ph.D. degree in Biochemical Engineering in 2019 from Huaqiao University. He is currently an assistant professor at the Institute of Biomaterials and Tissue Engineering at Huaqiao University, China. His research interests include the fabrication of 2D and 3D nanoframeworks for drug delivery, and molecular imaging, focusing on generating bio-inspired nanomaterials for cancer theranostics.*



**Ai-Zheng Chen**

*Ai-Zheng Chen received his Ph.D. degree in Biomedical Engineering from Sichuan University in 2007. After completing the postdoctoral research at The Hong Kong Polytechnic University, he joined Huaqiao University, where he is now a professor at the College of Chemical Engineering and Director of the Institute of Biomaterials and Tissue Engineering. His research interests mainly focus on micro- and nanoscale materials for drug delivery systems and tissue engineering.*



**Scheme 1** Schematic illustration of the construction principles, construction strategies, and biomedical applications of PMNMs.

findings of this review will provide a comprehensive understanding of these nanomaterials and offer guidance for their translation from the laboratory to clinical settings.

## 2. The construction principles and strategies of PMNMs

### 2.1. Construction principles

Unlike general mineralization, biomineralization stands out for its unique ability to control the orientation, nucleation, growth, and assembly of crystals from the molecular to the macroscopic levels through the interactions between organic macromolecules and inorganic ions at the interface. These consequences eventually result in the formation of organic–inorganic hybrid materials with distinctive hierarchical structures and assembly patterns. Two key aspects during biomineralization include the arrangement of organic macromolecules and their continuous interactions with inorganic minerals. Typically, biomineralization follows four stages: pre-assembly of the organic matrix, interfacial molecular recognition, modulation of crystal growth, and epitaxial growth of crystals.<sup>26</sup> During the biomineralization process, proteins act as an organic matrix, playing a key role in regulating the mineralization process of inorganic components. Research on the role of proteins in biomineralization mainly focuses on their func-

tions in nucleation and the growth of biominerals. Firstly, the pre-assembly of the organic matrix is a prerequisite for biomineralization. Before mineral deposition, proteins are pre-assembled in a specific manner to create an organized reaction environment. In this environment, these protein assemblies often act as the core of mineralized systems, providing sites for the nucleation of inorganic minerals and serving as a biological template to control the growth and assembly of crystals. Secondly, proteins influence the nucleation and growth of biominerals through molecular recognition at the organic–inorganic interface. Under the regulation of protein assemblies, inorganic components nucleate and grow at the organic–inorganic interface through various forces, including hydrogen bonds, electrostatic interactions, metal chelation, and van der Waals forces. The primary (amino acid sequences) and secondary (protein conformations, such as  $\alpha$ -helix and  $\beta$ -folding) structures of proteins are considered crucial in the molecular recognition process. The primary structure of proteins is essential for recognizing inorganic ions, as different amino acid residues can chelate various inorganic ions. The secondary structure of proteins can adapt to the molecular structure of inorganic crystals through conformational changes, facilitating molecular recognition. Molecular recognition at the organic–inorganic interface is a specific process that influences and regulates the crystal phase, crystal shape, orientation, and morphology of inorganic crystals.<sup>27</sup>

Recently, several efforts have been dedicated to the crystallization theory during biomineralization. The aggregate nucleation growth of monomers forms the theoretical basis of the classical crystallization model. This model helps understand the phenomena of crystallization promotion or inhibition and the equilibrium morphology of crystals in biomineralization and biomimetic mineralization systems. According to the classical nucleation theory, the original assembly units of crystals are atoms, ions, or molecules, and their growth accumulates on a stable crystal core through ion superposition and unit replication.<sup>28</sup> Various factors, including proteins, inorganic ions, and genes, influence the crystallization process of biominerals. Biomineralization is a complex mineral formation process that does not perfectly conform to the conventional nucleation theory of inorganic crystals. Studies have revealed the existence of other crystallization pathways in biomineralization systems, such as prenucleation clusters and disordered and amorphous precursor nucleation modes.<sup>29–32</sup> For example, Weiner *et al.* observed that the biomineralization process of spicules in sea urchin embryo consists of two stages.<sup>33</sup> Initially, it accumulates into a metastable transition phase through amorphous CaCO<sub>3</sub> nanoparticles (NPs) before

transforming into steady-state calcite single crystals. The formation of metastable amorphous precursors is a significant factor influencing the nucleation of CaP and CaCO<sub>3</sub> crystals. This transformation pathway is widespread in the formation of various biological minerals, including bones, teeth, and carapaces of animals.<sup>34–36</sup> Understanding the crystallization process in biomineralization research is crucial for an in-depth understanding of biomineralization processes and its regulatory mechanisms, as well for the design and preparation of active materials with biomineral-like structures and biogenic functions.

## 2.2. Construction strategies

Due to their unique structures, functions, and characteristics, proteins can serve as organic templates and stabilizers to guide and regulate the nucleation, growth, and assembly of inorganic components, resulting in the formation of NPs with uniform particle sizes. The wide variety of proteins and inorganic NPs provides diverse options for the construction of PMNMs. Depending on the type of proteins used, there are primarily two strategies: *in situ* mineralization and genetic engineering (Table 1).

**Table 1** Typical examples of nanomaterials prepared *via* protein-directed biomineralization and biomimetic mineralization technology

Strategy	Inorganic mineral	Protein	Nanomaterial	Size	Characteristic	Ref.
<i>In situ</i> mineralization	PtS	HSA	PtS-NDs	2.1 nm, 3.2 nm, 4.5 nm	Tunable size, excellent photothermal conversion performance, and effective resistance to photobleaching	39
	MnO <sub>2</sub>	BSA	MnO <sub>2</sub> NFs	50 nm (lateral size), 3 nm (thickness)	Remarkable tandem enzyme-like activities (GOx-like activity and peroxidase-like activity)	40
	Ag <sub>2</sub> S	BSA	Ag <sub>2–3x</sub> Bi <sub>x</sub> S QDs	4.1 nm	Desirable NIR-II fluorescence imaging capability and high photothermal conversion efficiency	77
	AuNCs	Keratin	AuNCs-Ag@Keratin-Gd	75 nm	Enhanced fluorescence intensity; high colloid stability	81
	CuCaP	GOx	PGC-DOX	88 ± 17 nm	H <sub>2</sub> O <sub>2</sub> self-supplying, GSH-eliminating properties, and efficient catalytic activity	105
	ZIF-8	GOx&HRP	GOx&HRP@ZIF-8/ASO	~ 410 nm	Superior biocompatibility and excellent anti-bacterial properties	115
Genetic engineering	Pt/Rh/Au/Ir/Mn	Genetically recombinant human heavy-chain ferritin	FTn-Pt/FTn-Rh/FTn-Au/FTn-Ir/FTn-Mn	2 nm/2 nm/2 nm/2 nm/6 nm	High peroxidase-like activity and effective tumor-targeting ability	52
	Co <sub>3</sub> O <sub>4</sub>	Genetically modified ferritin	HccFn(Co <sub>3</sub> O <sub>4</sub> )	12.1 ± 0.4 nm	Hcc-targeting ability and high peroxidase-like activity	56
	CoFe <sub>2</sub> O <sub>4</sub>	Genetically modified human ferritin	Co-doped HFT-MSH-NPs	~7 nm	Excellent melanoma-targeting ability and high hyperthermic efficiency	57
	Fe <sub>3</sub> O <sub>4</sub>	Genetically recombinant encapsulin	eMIONS	22 nm	Ultrahigh crystallinity, excellent magnetic-to-thermal conversion efficiency, and superior specific absorption rate	61
	Au	Genetically recombinant HSA	RHMH18@AuD NPs	80 nm	Tumor-targeting ability, enzyme-responsive drug release and favorable biocompatibility	63

Abbreviations: AuNCs – Gold nanoclusters; ASO – Antisense oligonucleotide; BSA – Bovine serum albumin; Ce6 – Chlorin e6; CuCaP – Copper-doped calcium phosphate; DOX – Doxorubicin; eMIONS – Encapsulin-produced magnetic iron oxide nanocomposites; Ftn – Ferritin; GOx – Glucose oxidase; GSH – Glutathione; Hcc – Hepatocellular carcinoma; HFT – Human ferritin; HRP – Horseradish peroxidase; HSA – Human serum albumin; MSH – Melanocyte-stimulating hormone peptide; NFs – Nanoflakes; NDs – Nanodots; NIR-II – Second near-infrared; PGC-DOX – PEG-GOx encapsulated and DOX-loaded CuCaP; QDs – Quantum dots; RHMH18@AuD NPs – HSA fusion protein NPs co-loaded with Au NPs and docetaxel; ZIF-8 – Zeolite imidazole framework-8.

**2.2.1. *In situ* mineralization strategy.** The interaction between metal ions and proteins mainly involves two main types: electrostatic interaction and metal reduction reaction. The primary structure of proteins is rich in a large number of active amino acid residues, such as negatively charged amino acid residues and redox-active amino acid residues,<sup>37</sup> which play a crucial role in the mineralization process of biominerals. They can act as nucleation sites for mineral that favor *in situ* mineral deposition. Specifically, negatively charged amino acid residues with carboxyl groups, like aspartate and glutamate, can combine with positively charged inorganic metal ions through electrostatic interactions. In the case of the supersaturated system, inorganic minerals can be formed spontaneously through ion adsorption and mineral deposition.<sup>38</sup> For instance, Li *et al.* applied human serum albumin (HSA) as a biological template to induce and regulate the biosynthesis of precious metal platinum sulfide nanodots (PtS-NDs).<sup>39</sup> PtS-NDs were synthesized in two steps: first, the Pt<sup>2+</sup>-HSA nanocomplex was formed through electrostatic interactions between the carboxyl group in HSA and Pt<sup>2+</sup> in PtCl<sub>2</sub>. Subsequent addition of Na<sub>2</sub>S in the solution promoted the nucleation and growth of PtS within the HSA cavity through a precipitation reaction. The particle size of PtS-NDs could be precisely controlled by adjusting HSA concentration and incubation time. PtS-NDs exhibited excellent photothermal conversion performance and resistance to photobleaching. Although the size and morphology of NPs can be adjusted by changing the preparation conditions, it is challenging to synthesize two-dimensional nanomaterials using albumin as a template. This may be due to the fact that albumin and inorganic crystals tend to form isotropic spherical structures under mild conditions, which is also present in nanomaterials synthesized by using other proteins as templates. Interestingly, Li *et al.* synthesized morphologically controllable MnO<sub>2</sub> nanoflakes (NFs) by adjusting the concentration of manganese ions using BSA as the nucleating skeleton and the stabilizer.<sup>40</sup> The lateral dimension of MnO<sub>2</sub> NFs could be adjusted by changing the concentration of BSA. In addition, the synthesized MnO<sub>2</sub> NFs exhibited excellent dual enzyme activities (glucose oxidase-like activity and peroxidase-like activity). Overall, this work provided a simple and effective strategy to synthesize two-dimensional metal oxide nanomaterials utilizing a protein-directed biomineralization.

*In situ* mineralization of minerals, such as CaP, manganese phosphate, or copper phosphate on the glucose oxidase (GOx) template, can be achieved by adding GOx and inorganic metal ions (*e.g.*, calcium, manganese, or copper ions) to a sugar-free, phosphate-rich DMEM solution with pH buffering capacity (pH = 7.4).<sup>41</sup> For example, Huang *et al.* prepared a manganese-doped CaP NPs through a biomimetic mineralization strategy. Then, catalase (CAT) and sinoporphyrin sodium were co-encapsulated on the surface of the NPs by simple mixing. Thus, a biodegradable and O<sub>2</sub> self-supplying nanoplatform (named GMCD) was obtained.<sup>42</sup> The GMCD exhibited good biocompatibility, a long-term sustained drug release, and an excellent tumor growth-suppressed effect. In addition to the ion adsorption and deposition, the coordination effect between metal ions and

organic ligands contributes to the nucleation and growth of minerals on protein templates.<sup>43</sup> For instance, Chen *et al.* proposed a general and rapid biomimetic mineralization strategy for efficiently delivering proteins by mixing different proteins (*e.g.*,  $\beta$ -galactosidase, caspase 3/HSA, BSA, and ferritin) with 2-methyl imidazole (2-MI) and subsequently adding a zinc nitrate solution.<sup>44</sup> Due to the high affinity of Zn<sup>2+</sup> to proteins and the strong coordination effect between Zn<sup>2+</sup> and 2-MI, biomineralized zeolitic imidazolate framework-8 (ZIF-8) NPs were successfully synthesized. This approach preserved the biological activity of the protein and protected it from degradation by proteolytic enzymes. Furthermore, with polymer modification, the ZIF-8 NPs could achieve long-term storage in the culture medium without significant activity loss.

In addition, the surface of proteins is typically rich in redox-active amino acid residues, such as tyrosine, tryptophan, and cysteine.<sup>45</sup> These amino acid residues exhibit strong reduction abilities, allowing them to adsorb metal ions such as manganese, platinum, gold, and silver ions, enabling the reduction of high-valent metal ions to low-valent metal ions, which is conducive to the nucleation and growth of inorganic nanomaterials. During this process, proteins serve not only as biological templates but also as reducing agents. For instance, the potent oxidant KMnO<sub>4</sub> undergoes a rapid redox reaction when in contact with organic substances. The resulting reduction product then further reacts with the protein to generate a protein-MnO<sub>2</sub> complex. Emulating this intriguing process, Pan *et al.* introduced an exceptionally straightforward strategy for preparing multifunctional protein-MnO<sub>2</sub> NPs.<sup>46</sup> Specifically, by employing BSA as both the reducing agent and template, they synthesized BSA-MnO<sub>2</sub> NPs through a redox reaction involving KMnO<sub>4</sub> and BSA in an aqueous solution, stirring at 37 °C for 2 hours. BSA-MnO<sub>2</sub> NPs exhibited uniform size (2.9 nm), excellent monodispersity, and good T<sub>1</sub> relaxation performance (7.9 mM<sup>-1</sup> s<sup>-1</sup>). Furthermore, two nanoprobe, BMP and BMI, were created for MRI-guided chemotherapy and photothermal therapy (PTT) by simply incorporating two drugs, paclitaxel and indocyanine green (ICG), into the hydrophobic domain of BSA within BSA-MnO<sub>2</sub> NPs. Similarly, this strategy could be equally applicable to the preparation of other protein-based nanoprobe, such as ovalbumin and transferrin. While biomineralization strategies hold great potential in producing multifunctional nanotheranostic agents by thoughtfully integrating biological macromolecules and inorganic materials, it is important to note that the effective and reproducible preparation of such nanotheranostic agents remains a challenge. In this regard, Xiao *et al.* applied oxidative polymerization in the biomineralization process of the albumin template, enabling the simple synthesis of nanotheranostic drugs.<sup>47</sup> They synthesized a series of biomineralized polymers and MnO<sub>2</sub> mixed NPs (PMHNs) by polymerizing different monomers, such as dopamine (DA), pyrrole (PY), and epigallocatechin (EGC), and reducing KMnO<sub>4</sub> within an albumin template. These PMHNs exhibited good biocompatibility and renal clearance and possessed an ultra-high longitudinal relaxation (r<sub>1</sub>, 38.14 mM<sup>-1</sup> s<sup>-1</sup>) and excellent photothermal conversion

efficiency (47.1%). In summary, combining oxidative polymerization and biomineralization strategies offered a feasible approach for the straightforward and reproducible preparation of multifunctional nanotheranostic agents.

**2.2.2. Genetic engineering strategy.** The presence of a structure that induces ion nucleation and a space that limits the maximum growth of crystals is essential for achieving directed biomineralization.<sup>48</sup> Ferritin, a vital protein naturally occurring in various eukaryotes, self-assembles from heavy and light chains into a spherical cage structure with an outer diameter of 12 nm and an inner diameter of 8 nm, responsible for iron transport and storage within the body.<sup>49,50</sup> Ferritin nanocages are the most extensively studied proteins in iron metabolism and serve as a representative system for studying biomineralization both *in vivo* and *in vitro*. Given the presence of ferroxidase centers (FOCs), ferritin possesses a natural biomineralization capacity, making it a powerful tool for the synthesis of various metal nanoclusters (NCs), and metal oxide NPs, including AuNCs,<sup>51</sup> PtNCs,<sup>52</sup> Co<sub>3</sub>O<sub>4</sub> NPs,<sup>53</sup> and MnO<sub>2</sub> NPs.<sup>54</sup> Although ferritin nanocages can be targeted by combining them with the transferrin receptor 1 (TfR1), achieving more diverse and precise targeting modifications on the ferritin surface is necessary to enhance their targeting effectiveness and broaden biomedical applications. Ferritin is amenable to specific modifications through genetic engineering techniques, enabling functionalization of the nanocage's surface with targeted peptides, such as Arg-Gly-Asp (RGD) peptide,<sup>55</sup> hepatocellular carcinoma cell-specific peptide SP94,<sup>56</sup> and melanocyte-stimulating-hormone peptide.<sup>57</sup> These functional modifications provide ferritin with cell-specific targeting abilities to enhance the utilization and therapeutic effectiveness of ferritin-based nanomedicine while reducing side effects on non-target organs. Without interfering with the unique structure of the ferritin nanocage, the Douglas research group used genetic engineering techniques for the first time to modify the surface of human H-chain ferritin (HFn) with the targeted RGD polypeptide (RGD-4C peptide) in 2006, resulting in the creation of RGD4C-Fn.<sup>55</sup> Subsequently, RGD4C-Fn was employed as a biological template for *in vitro* biomimetic mineralization to synthesize magnetite NPs. The genetically-engineered RGD4C-Fn exhibited improved tolerance and could guide the mineralization process of magnetite NPs at a higher temperature (65 °C) and pH (8.5) compared to the control group (HFn). Furthermore, magnetite NPs derived from RGD4C-Fn mineralization demonstrated enhanced cell-specific targeting capabilities to target  $\alpha_v\beta_3$  integrins on angiogenic tumor vasculature. This work represented an innovative expansion of the application of protein nanocages in cancer therapy. The combined approach of protein nanocages and genetic engineering techniques could be applied to the surface modification of other protein nanocages and the incorporation of other peptides into protein nanocages.

Unlike ferritin, encapsulin is an iron-storage protein discovered in prokaryotes in recent years. It has a larger size and greater loading capacity than ferritin. Despite its different origin, it shares a functional sequence similarity of 70% with

ferritin and possesses the same FOCs.<sup>58,59</sup> However, iron-storage protein nanocages form NPs only through the spontaneous biomineralization processes of organisms, which suffers from several disadvantages, such as low mineralization efficiency and inadequate performance. Genetic recombinant protein has gained significant attention in recent years in nanomedicine research.<sup>60</sup> Genetic engineering modifications can enhance the biomineralization abilities of iron-storage proteins, yielding NPs with superior performance. Zhang *et al.* utilized genetic engineering technology to modify the iron-storage protein encapsulin from *Myxococcus xanthus*, re-engineering three proteins, such as encA, encB, and encC.<sup>61</sup> The expression levels of encB and encC, the major proteins responsible for mineralization, were approximately two-fold higher than those in the wild-type encapsulin. Subsequently, they employed biomimetic mineralization technology to fabricate encapsulin-produced magnetic iron oxide nanocomposites (eMIONS). Given the high expression levels of encB and encC, eMIONS exhibited a crystallinity of up to 100%. Furthermore, eMIONS in the presence of a magnetic field demonstrated excellent magnetic-to-thermal conversion efficiency and a superior specific absorption rate (SAR). The SAR value of eMIONS reached up to 2390 W g<sup>-1</sup>, which was nearly 20-fold higher than that of the clinically used IONs Feridex (115 W g<sup>-1</sup>). This work effectively addressed the issue of low magnetic-to-thermal conversion in magnetic hyperthermia therapy to a significant extent.

Using genetic engineering, specific sequences can be inserted into the gene sequences of proteins, allowing the generation of multifunctional proteins. Then, these newly engineered proteins are expressed by bacteria, thus realizing precise modification of protein structures. In addition to the ferritin family, HSA can be genetically engineered to produce customized multifunctional HSA fusion proteins. For instance, Chen *et al.* used gene fusion technology to modify HSA by introducing poly-histidine, matrix metalloproteinase-2 (MMP-2) response sites, and RGD peptides at the C- and N-termini of HSA, respectively.<sup>62</sup> A fusion protein named RHMH18 was then expressed by *Pichia pastoris*, integrating pH responsiveness, MMP-2 enzyme responsiveness, and tumor targeting. Furthermore, ultrasmall Au NPs were embedded into the RHMH18 protein through biomimetic mineralization, while chemotherapeutic docetaxel was loaded into histidine micelles through hydrophobic interactions, resulting in the formation of RHMH18@AuD NPs.<sup>63</sup> The conformation of RHMH18@AuD NPs remained consistent with native HSA, ensuring the excellent biocompatibility of the NPs. Combined with near-infrared (NIR) laser irradiation, RHMH18@AuD NPs achieved highly effective treatment for ovarian cancer by leveraging the synergistic effects of chemotherapy and PTT.

### 3. Biomedical applications

Generally speaking, proteins possess some characteristics such as good biocompatibility, stability, targeting, and multifunc-

tionality. Some inorganic components might have excellent performance in optics, heat, or magnetism. Owing to their comprehensive performances, these PMNMs nanocomposites hold great potential in biomedical applications. Next, we focus on the recent progress of PMNMs in bioimaging, anti-tumor therapy, anti-bacterial therapy, and anti-inflammatory therapy. These nanomaterials encountering potential obstacles in their applications, as well as the opportunities, are also discussed. Hopefully, new insights and inspirations are provided for the development of new PMNMs.

### 3.1. Bioimaging

Modern biomedical imaging technologies are crucial in all stages of biomedical disease management, including prevention, diagnosis, grading, prognosis, and surgical guidance.<sup>64</sup> The versatile application of imaging techniques allows the study of physiological and pathological processes objectively, spanning multiple scales of time and space. Organic-inorganic nanomaterials synthesized through protein-directed biomineralization are ideal for bioimaging applications. They can be structurally modified using genetic engineering or chemical reactions, and they offer the flexibility to serve as the mineralization chamber for heavy atoms or metal complexes mineralization compartments and incorporate probe molecules.<sup>65</sup> These properties make PMNMs highly promising in the field of biological imaging applications, applicable to magnetic resonance imaging (MRI), fluorescence imaging (FI), and bimodal imaging.

**3.1.1. Magnetic resonance imaging (MRI).** MRI is a non-invasive diagnostic technique that is widely used due to its excellent temporal and spatial resolution.<sup>66</sup> Excellent MRI contrast agents are crucial to achieving MRI. However, most contrast agents have poor selectivity, low proton relaxation, and high toxicity after administration. With biomineralization or biomimetic mineralization technology, proteins can be easily synthesized *in vitro* metal oxide nanomaterials, like  $\text{MnO}_2$ ,<sup>67</sup>  $\text{Gd}_2\text{O}_3$ ,<sup>68</sup> and  $\text{Fe}_3\text{O}_4$ ,<sup>69</sup> by adsorbing magnetic elements (e.g.,  $\text{Mn}^{2+}$ ,  $\text{Gd}^{3+}$ , and  $\text{Fe}^{3+}$ ). These composite nanomaterials usually have excellent imaging contrast and are biocompatible, thus they are expected to be employed as MRI contrast agents. In the case of albumin, its mineralization chamber can be used as a “foundry” for the synthetics of metal oxide nanomaterials, and its high affinity to albumin receptors and easy modification make albumin NPs potential candidates for tumor MRI. Wang *et al.* synthesized ultra-paramagnetic iron oxide NPs (uBSPIOs) through a one-step *in situ* mineralization strategy by using BSA as a template.<sup>70</sup> uBSPIOs have a good monodispersity and an ultra-high transverse relaxation ( $444.56 \pm 8.82 \text{ mM}^{-1} \text{ s}^{-1}$ ). uBSPIOs also have an extremely high saturation magnetization ( $84.32 \text{ emu g}^{-1}$ ), much higher than other  $\text{Fe}_3\text{O}_4$  NPs of the same size.<sup>71</sup> After coupling luteinizing hormone-releasing hormone peptide on the surface of uBSPIOs, tumor targeting can be achieved, and  $T_2$ -weighted MRI can be realized. By combining the pathological characteristics of the lesion microenvironment, microenvironment-responsive contrast agents can be designed to perform precise

MRI of the lesion site. Considering the acidic microenvironment of acute myocardial infarction (AMI) disease, Wang *et al.* prepared a pH-responsive and biocompatible nanoprobe ( $\text{MnO}_2$ @BSA) for  $T_1$ -weighted MRI of AMI in the rabbit model (Fig. 1a-i).<sup>72</sup> Compared with the low  $r_1$  ( $0.34 \text{ mM}^{-1} \text{ s}^{-1}$ ) under normal physiological conditions (pH 7.4),  $\text{MnO}_2$ @BSA showed an acidic pH-responsive  $\text{Mn}^{2+}$  release behavior with molecular relaxation of about 38-fold and 55-fold improvement in simulating the AMI environment (pH 6.5) and the intracellular environment of macrophages (pH 5.0), respectively. In addition,  $\text{MnO}_2$ @BSA could be selectively enriched in AMI tissues in a short time and detected AMI in heart tissue for diagnosis. The contrast enhancement was significantly better than commercially available Gd-DTPA ( $4.3 \text{ mM}^{-1} \text{ s}^{-1}$ ) and  $\text{Gd}_2\text{O}_3$ @BSA without the pH-responsive characteristics (Fig. 1a-ii). The results showed that nanoprobe with pH-responsive properties greatly improved the sensitivity and specificity for early diagnosis of focal tissues, which is achieved by significantly amplifying the imaging contrast of focal tissue and switching the imaging signal.

**3.1.2. Fluorescence imaging (FI).** As an important tool for preclinical research, FI can accurately identify and report on diseases. Nowadays, two materials are mainly used for FI. One of them is biological materials, such as fluorescent proteins;<sup>73</sup> the other is inorganic and organic fluorescent materials, such as quantum dots<sup>74</sup> and carbon nanotubes.<sup>75</sup> However, these materials suffer from disadvantages such as poor stability and poor biocompatibility. Some inorganic nanomaterials with fluorescence characteristics can be produced through biomineralization and biomimetic mineralization strategies on the basis of protein, such as  $\text{Ag}_2\text{S}$  NCs,<sup>76,77</sup> CdNCs,<sup>78</sup> and AuNCs.<sup>79</sup> These materials offer relatively good biocompatibility and *in vivo* stability. Since histidine on the ferritin heavy chain can bind metal ions, excited AuNCs were synthesized inside ferritin by Sun *et al.*<sup>80</sup> By measuring the fluorescence spectrum, the energy resonance transfer between the two AuNCs with increasing size and decreasing distance between the two gold clusters would gradually increase the total fluorescence intensity of the two nanoclusters and redshift the fluorescence spectrum. They successfully performed targeted FI in Caco-2 cells with the ferritin receptor and in the kidneys of mice, respectively. AuNCs synthesized as protein templates have attracted much attention in FI due to their simple synthesis and good biocompatibility. However, these nanomaterials still have problems such as poor colloidal stability and nonideal fluorescence intensity. A self-assembly strategy of cation-induced protein-AuNCs for enhanced FI was proposed by Li *et al.* (Fig. 1b-i).<sup>81</sup> Firstly, they synthesized AuNCs using cysteine-rich keratin as a template. After silver ions modification and Gd ions doping of AuNCs@Keratin, AuNCs-Ag@Keratin-Gd was obtained. The colloidal stability of the NPs was improved due to the blocking of free thiols in keratin. Storage in aqueous solution for up to four months, with negligible changes in hydrodynamic diameter. In addition, after four months of storage, AuNCs-Ag@Keratin-Gd could still maintain more than 85% of the fluorescence intensity, which

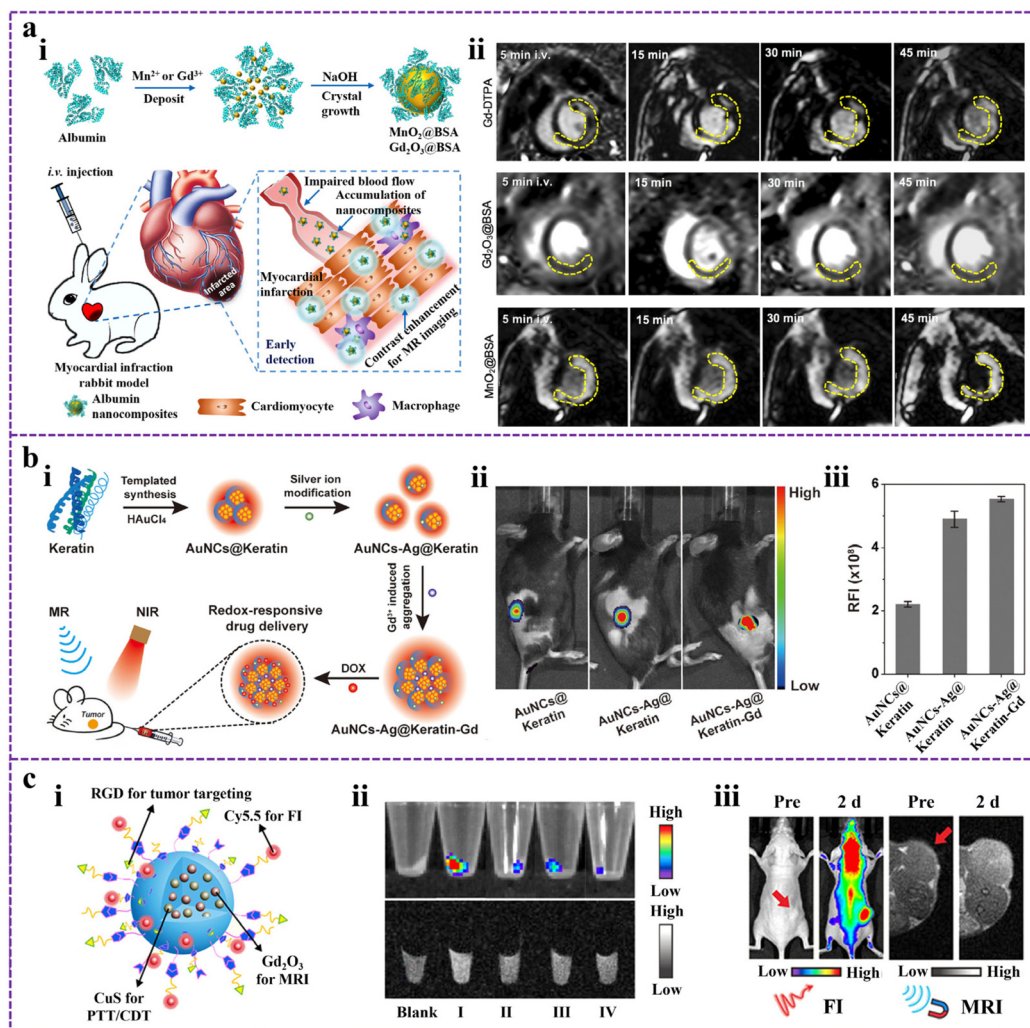


**Fig. 1** (a) The biomimetic nanocomposites for precise MRI. (i) Schematic of MnO<sub>2</sub>@BSA and Gd<sub>2</sub>O<sub>3</sub>@BSA nanocomposites for conducting MRI of AMI in rabbit models. (ii) MRI of AMI in rabbits contrasted by Gd-DTPA, Gd<sub>2</sub>O<sub>3</sub>@BSA, and MnO<sub>2</sub>@BSA. Reproduced from ref. 72 with permission. Copyright 2020. Elsevier. (b) Keratin-templated gold nanoclusters (AuNCs@Keratin) for enhanced FI. (i) The construction process of dual-metal doped AuNCs@Keratin (AuNCs-Ag@Keratin-Gd) and their applications in biomedical fields. (ii) FI images of 4T1 tumor-bearing mice after administering different samples. (iii) Relative fluorescence intensities were measured from the image in (ii). Modified from ref. 81 with permission. Copyright 2020. Elsevier. (c) A BSA-mineralized nanoprobe for *in vivo* bimodal imaging. (i) Structural illustration of BCGCR. (ii) FI images (top) and MRI images (bottom) of cell pellets (Blank: Untreated cells; I: U87MG cells treated with BCGCR; II: U87MG cells treated with BCGC; III: U87MG cells treated with RGD first, followed by the addition of BCGCR; IV: HEK293T cells treated with BCGCR). (iii) *In vivo* FI images and MRI images of tumor-bearing mice after intravenous injection of BCGCR. Reproduced from ref. 87 with permission. Copyright 2022. American Chemical Society.

was in sharp contrast to the results of AuNCs@Keratin (the fluorescence intensity is maintained at about 60% of the initial after four weeks of storage). Silver ions modification effectively increased the fluorescence intensity of the NPs, which was mainly attributed to the “silver effect”.<sup>82,83</sup> The fluorescence intensity of AuNCs-Ag@Keratin particles was further enhanced to 6.5 times that of AuNCs@Keratin upon Gd ions-induced aggregation. The excellent FI performance of nanocomposite was also validated by *in vivo* FI experiments in mice (Fig. 1b-ii and iii).

**3.1.3. Bimodal imaging.** With the development of science and technology, a single imaging modality may not meet the demand for accurate detection of patients' diseases. For

example, FI techniques, despite their high sensitivity and selective excitation, also have the disadvantages of poor spatial resolution and low optical tissue penetration depth, so they are mostly limited at the animal level.<sup>84</sup> Although there are several clinical examples of surgical navigation through optical imaging, fluorescent substances have poor resistance to photobleaching and are easily cleared by the body, greatly hampering their applicability.<sup>85</sup> Therefore, multimodal imaging technology has emerged to realize the complementary advantages of multiple imaging technologies. For the same lesion area, different imaging modes and fusion analyses are combined to obtain more accurate pathological results, which greatly improves the sensitivity and accuracy of imaging detec-



tion and also helps doctors to make more accurate decision.<sup>86</sup> Using BSA as the template and the stabilizer, Luo *et al.* synthesized CuS/Gd<sub>2</sub>O<sub>3</sub> NPs (named BCG) with an average size of 5 nm through a biomimetic mineralization strategy.<sup>87</sup> The Cy5.5 fluorophore and RGD peptide were further modified on the surface of BCG to fabricate a tumor-targeted nanoprobe (named BCGCR) (Fig. 1c-i). The modified RGD peptide endowed BCGCR with the ability to actively recognize tumor cells, as well as facilitated the uptake of BCGCR by tumor cells (Fig. 1c-ii). The BCGCR could be applied for MRI/FI bimodal imaging of tumors with high spatial resolution and high sensitivity (Fig. 1c-iii). In terms of fluorescence properties, the BCGCR could emit strong NIR fluorescence at 710 nm. For MRI, the BCGCR possessed a high longitudinal relaxation at 1.5 T ( $r_1 = 15.3 \text{ mM}^{-1} \text{ s}^{-1}$ ), which was 3-fold higher than that of the clinically used Gd-DTPA ( $r_1 = 4.3 \text{ mM}^{-1} \text{ s}^{-1}$ ). The improved longitudinal relaxation might be attributed to the fact that Gd was encapsulated within the limited space of BSA, hindering the rotation and thus prolonging the tumbling time. Based on these satisfactory performances, BCGCR might have great potential for bimodal imaging as both a sensitive FI probe and an effective  $T_1$ -weighted MRI contrast agent.

### 3.2. Anti-tumor therapy

In recent years, the increasing incidence and mortality of cancer have become a serious threat to human health and life, and effective cancer treatment has become a major challenge in the field of medical research.<sup>88,89</sup> At present, surgery, chemotherapy, and radiotherapy are the most commonly used cancer treatment methods clinically. However, these traditional treatments still have many shortcomings, including non-specific treatment, ease of metastasis and recurrence, acquired multidrug resistance, and serious toxic side effects.<sup>90-92</sup> With the development and rise of nanomedicine, the drawbacks of traditional cancer therapy are expected to be overcome. Through the enhanced permeability and retention effect (EPR) of solid tumors or surface coupling of targeting ligand, nanocarriers can realize the selective administration of tumor tissue by passive or active targeting to improve the bio-availability of anti-cancer drugs, enhance the therapeutic effect, and reduce the toxic side effects.<sup>93-95</sup> Compared with chemical methods to prepare nanocarriers, mineralization-based methods are characterized by good biocompatibility, facile nature, and low cost, having high feasibility and great potential from laboratory research to clinical application. Moreover, tumor tissues showed significantly different physiological properties, such as slight acidity, hypoxia, GSH overexpression, and enzyme overexpression.<sup>96-98</sup> Based on these characteristic pathological signals, the researchers constructed numerous nanocarriers in response to the tumor microenvironment (TME). These vectors can undergo structural or conformational changes in response to endogenous stimuli such as pH, GSH, and enzymes, which can trigger the precise and controlled release of the loaded drugs. For instance, Xie *et al.* used BSA-biomaterialized MnO<sub>2</sub> as a carrier for loading the anti-tumor drug methotrexate (MTX) and fluorescent dye Cy5.5

through amide condensation, to prepare the nanodrug MTX-BSA@MnO<sub>2</sub>-Cy5.5 (MBMC NPs).<sup>99</sup> The designed MBMC NPs are for the diagnosis and treatment of anaplastic thyroid carcinoma. MBMC NPs showed good pH-responsive drug release and imaging performance. Specifically, the drug release experiment showed that the cumulative release rate of MBMC NPs reached 88.84% at pH-5.5 in 48 hours, which was much higher than the cumulative release rate at pH-7.4 (57.09%). This result could be conducive to achieving the targeted release of MTX from nanomedicine at the tumor site and to a lower extent in normal tissues, thus ensuring the therapeutic efficacy and safety of nanomedicine. With the rapid development of cancer therapy, a variety of novel cancer therapeutic modalities have been developed, such as PTT, photodynamic therapy (PDT), and chemodynamic therapy (CDT), except chemotherapy, radiotherapy, and surgery.<sup>100,101</sup> Combining the chemotherapy mediated by the nanodrug delivery systems with these advanced therapeutic modalities can further enhance the tumor growth-suppressed effect and even achieve complete tumor eradication. In another example, Xue *et al.* reported a multiple stimuli-responsive drug-loaded nanoplatform using silk fibroin as a template and a reducing agent.<sup>102</sup> Due to acidity-triggered MnO<sub>2</sub> degradation and protonation of the amino groups in doxorubicin (DOX), the accelerated release of DOX is achieved. The addition of H<sub>2</sub>O<sub>2</sub> also induced SMID NPs to release more DOX. In addition, the increased temperature helps to increase the release rate of DOX from SMID NPs. This may be attributed to the destruction of ICG/DOX complex and the increase in DOX solubility. The result of *in vivo* anti-tumor experiments showed that the nanoplatform could realize the combination of PTT, PDT, and chemotherapy, with the best inhibitory effect on 4T1 tumor growth.

Among various cancer therapeutic modalities, CDT is an effective therapeutic modality that kills tumor cells by catalyzing the production of highly toxic ·OH by endogenous H<sub>2</sub>O<sub>2</sub>.<sup>103,104</sup> However, insufficient H<sub>2</sub>O<sub>2</sub> in tumor cells and high glutathione (GSH) concentrations limit the efficacy of CDT. Accordingly, Huang *et al.* designed an intelligent nanomedicine with H<sub>2</sub>O<sub>2</sub> self-supplying and GSH-eliminating properties (Fig. 2a).<sup>105</sup> Copper-doped CaP NPs were prepared by one-step biomineralization using polyethylene glycol-modified GOx as a template. After loading the anti-tumor drug DOX, a well-monodispersed PGC-DOX NPs was obtained (Fig. 2b). In response to the acidic TME, PGC-DOX NPs were disintegrated, releasing payloads such as GOx, Cu<sup>2+</sup>, and DOX. GOx could effectively catalyze glucose to produce H<sub>2</sub>O<sub>2</sub> (Fig. 2c), which not only starved cancer cells but also provided substrates for the subsequent Fenton-like reaction. The released Cu<sup>2+</sup> underwent a redox reaction with intracellular GSH, resulting in GSH depletion, and simultaneous reduction of Cu<sup>2+</sup> to the Fenton-like reagent Cu<sup>+</sup>. Further, large amounts of ·OH were generated through the Cu<sup>+</sup>-mediated Fenton-like reaction for efficient CDT (Fig. 2d). By integrating GOx-mediated starvation therapy, Cu<sup>+</sup>-mediated CDT, and DOX-mediated chemotherapy, PGC-DOX could effectively inhibit the fast growth of 4T1

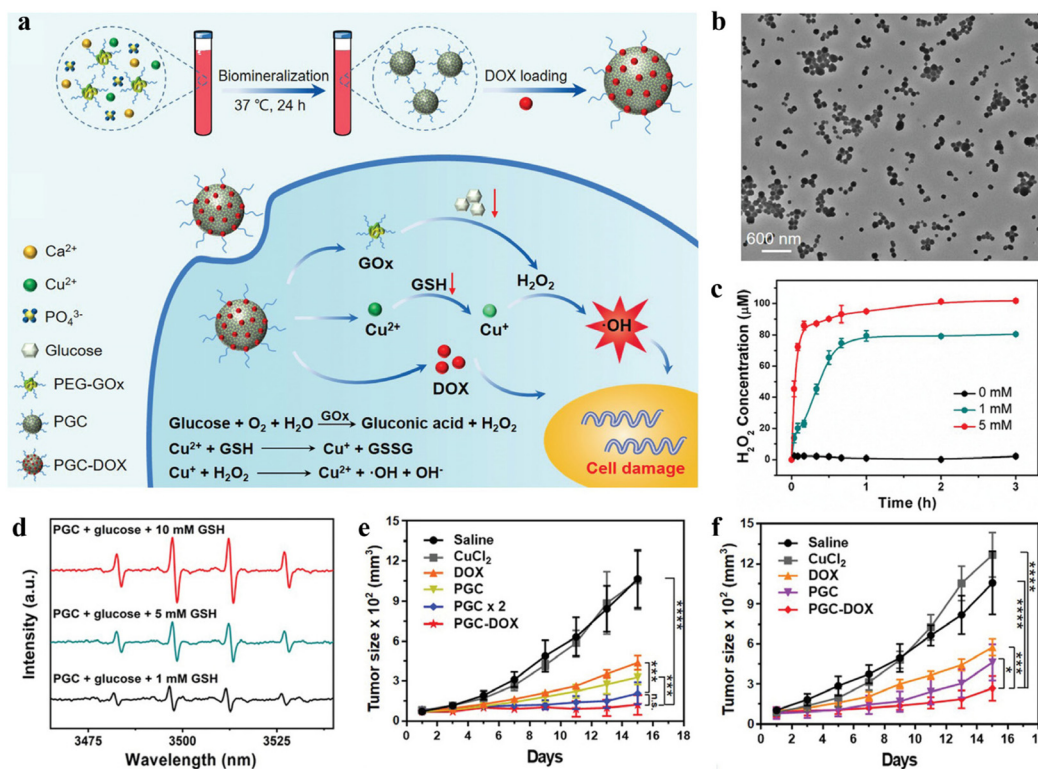


**Fig. 2** An intelligent nanoplatform constructed by *in situ* mineralization of GOx and its application in synergistic cancer therapy. (a) Schematic representation of the preparation of PGC-DOX and its therapeutic mechanism of cooperative cancer therapy. (b) TEM image of PEG-DOX. (c) Generated H<sub>2</sub>O<sub>2</sub> levels of PGC-DOX after incubation with different concentrations of glucose. (d) The ·OH production was examined by electron spin resonance spectra. (e) Relative tumor volume of 4T1-tumor-bearing mice treated by intratumoral administration. (f) Relative tumor volume of 4T1-tumor-bearing mice treated by intravenous injection. Reproduced from ref. 105 with permission. Copyright 2021. Wiley-VCH GmbH.

tumors, not only through intratumoral injection (Fig. 2e) and intravenous injection (Fig. 2f).

### 3.3. Anti-bacterial therapy

Since the introduction of antibiotics in the mid-20<sup>th</sup> century, the fatality rate of bacterial infectious diseases has dropped dramatically. However, with the large-scale abuse of antibiotics in recent years, bacteria have gradually developed resistance to traditional antibiotics, resulting in the emergence of the so-called “superbug”.<sup>106,107</sup> Moreover, bacteria can protect themselves from exogenous substances such as antibiotics by forming biofilms. The bacteria in the biofilm are significantly different from the free strain in terms of morphological and physiological roles, and their tolerance to antibiotics will be significantly improved.<sup>108</sup> The combination of these two adverse factors significantly improves bacterial resistance to antibiotics, weakens the effectiveness of conventional anti-bacterial treatment, and triggers intractable infectious diseases. To address the growing problem of bacterial drug resistance, it is urgent to develop new and effective anti-bacterial strategies to replace traditional anti-bacterial therapies for the treatment of drug-resistant bacterial infectious diseases. Nanomaterial-based therapeutics are considered to be an effective approach to combating recalcitrant bacterial infections, effectively

killing drug-resistant bacteria without causing an increase in drug resistance.<sup>109</sup> Recently, nanomaterials prepared based on biomineralization and biomimetic mineralization techniques were also used to combat bacterial infections due to their good biocompatibility and excellent anti-microbial properties. Through biomineralization technology, some inorganic nanomaterials with anti-bacterial performance can be easily and quickly synthesized, such as Ag NPs,<sup>110</sup> Au NPs,<sup>111</sup> Cu<sub>2</sub>O NPs,<sup>112</sup> and other nanomaterials. Adjusting the particle size and surface functionalization can strengthen the interactions between nanomaterials and bacteria, interfering with the communication between bacteria (*i.e.*, quorum sensing),<sup>113</sup> and hindering the formation of biofilm. Nanomaterials prepared based on biomineralization and biomimetic mineralization techniques may provide an effective strategy to solve the global problem of bacterial drug resistance.

*Staphylococcus aureus* (*S. aureus*) and *Escherichia coli* (*E. coli*) are the most common pathogenic bacteria. Huang *et al.* prepared copper sulfide (CuS) NPs with a uniform size utilizing BSA as a template.<sup>114</sup> The as-formed BSA-CuS nanomaterials exhibited good biocompatibility and low toxicity to the normal cells. In addition, under 980 nm laser irradiation, BSA-CuS nanomaterials showed excellent photothermal performance and a strong ability to ablate pathogenic bacteria.

Specifically, BSA-CuS nanomaterials could kill more than 80% of the bacteria (*S. aureus* or *E. coli*) at a low CuS concentration (50 ppm). Due to their facile preparation, low cost, and high photothermal conversion efficiency, the combination of BSA-CuS nanomaterials with NIR laser irradiation provided a very promising strategy for perishing drug-resistant strains. In another study, Zhang *et al.* used biomimetic mineralization and electrostatic interactions to construct a ZIF-8 nanocomposite (GOx&HRP@ZIF-8/ASO) through encapsulating biological cascade enzymes (GOx, and horseradish peroxidase, HRP) and adsorbing ftsZ antisense oligonucleotides (ASO), to combat drug-resistant bacterial infections (Fig. 3a).<sup>115</sup> The preparation process of the nanomaterials was relatively mild and simple, which could avoid the loss of GOx and HRP activities. They were embedded in the inner cavity of ZIF-8 with a high encapsulation efficiency of GOx (63.62%) and HRP (91.46%). The *in vitro* anti-bacterial experiments results indicated that GOx&HRP@ZIF-8/ASO NPs exhibited excellent anti-bacterial efficacy and strong biofilm destruction against methicillin-resistant *S. aureus* (MRSA), with the minimum inhibitory

concentration of  $16 \mu\text{g mL}^{-1}$ . These results could be attained by integrating the anti-bacterial effect of  $\cdot\text{OH}$  produced by cascade enzyme reaction and the inhibitory effect of the ftsZ gene by ftsZ ASO. The removal efficiency of MRSA biofilm could reach 88.2%, which was much higher than the efficiency of ZIF-8 (32.85%) and ftsZ ASO (58.65%). Furthermore, the *in vivo* anti-bacterial activity was investigated using a mouse model of wound infections caused by MRSA. The results demonstrated that the synergistic anti-bacterial system exhibited potent bactericidal effects and wound-healing performance (Fig. 3b and c). Overall, this study filled a gap in the anti-bacterial applications of biological enzymes and provides a potential therapeutic strategy for curing drug-resistant bacterial infections.

### 3.4. Anti-inflammatory therapy

Inflammation is a positive biological response of the body to the exogenous pathogens or the endogenous stimuli. It is a natural defense mechanism of the body, a process of removing harmful substances and initiating the self-healing of the

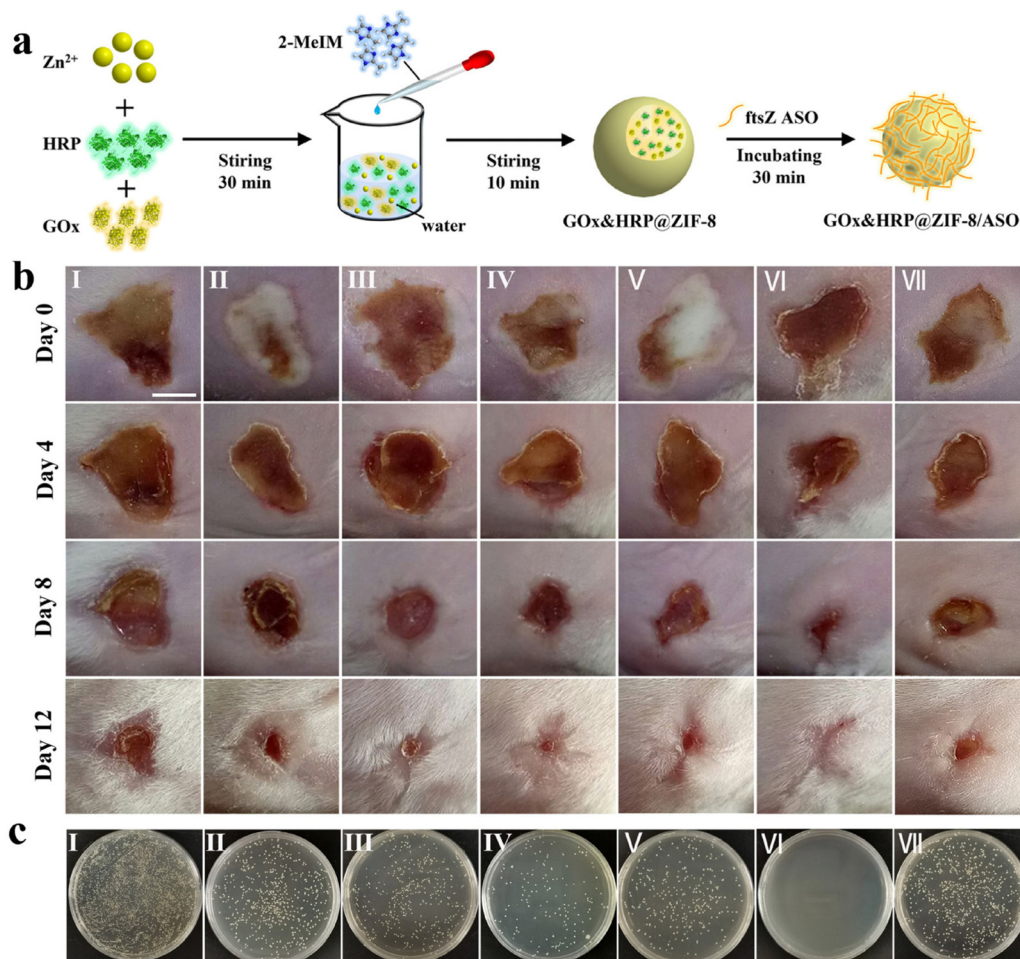


**Fig. 3** Biomineralized ZIF-8 nanomaterial for anti-bacterial therapy. (a) Illustration of the construction of GOx&HRP@ZIF-8/ASO NPs. (b) The pictures of MRSA-infected skins. (c) Photographs of MRSA colonies isolated from the infected wounds of mice after receiving different treatments (I: Saline, II: ZIF-8, III: GOx&HRP@ZIF-8, IV: GOx&HRP@ZIF-8 + Glu, V: GOx&HRP@ZIF-8/ASO, VI: GOx&HRP@ZIF-8/ASO + Glu, VII: ftsZ ASO). Reproduced from ref. 115 with permission. Copyright 2022. American Chemical Society.

body.<sup>116</sup> However, the long-term and uncontrolled inflammatory response tends to induce the occurrence of many diseases, including cardiovascular diseases, neurodegenerative diseases, and various inflammatory diseases.<sup>117,118</sup> Inflammatory diseases include inflammatory bowel diseases, arthritis, and pancreatitis, which cause a high economic burden on society. Moreover, increasing studies have suggested that oxidative stress occupies an important role in the progression of these inflammatory diseases.<sup>119</sup> The main medications used currently to treat inflammatory diseases include steroids, non-steroidal anti-inflammatory drugs, and immunosuppressants. The use of these traditional drugs, although effective, tended

to cause some unnecessary side effects, such as hemolytic anemia and osteoporosis.<sup>117,120</sup> Compared with the traditional drugs, NPs can integrate anti-inflammatory, anti-oxidation, and immunomodulation, achieving ideal therapeutic results with lower toxic side effects. PMNMs have been extensively applied to improve the therapeutic efficacy and safety of NPs for the treatment of inflammatory diseases.

Inflammatory bowel disease (IBD) is a chronic bowel disease characterized by alternating episodes of recurrence and remission, with major types including ulcerative colitis and Crohn's disease.<sup>121</sup> The etiology and pathogenesis of IBD are complex and unclear. Among the various pathologic

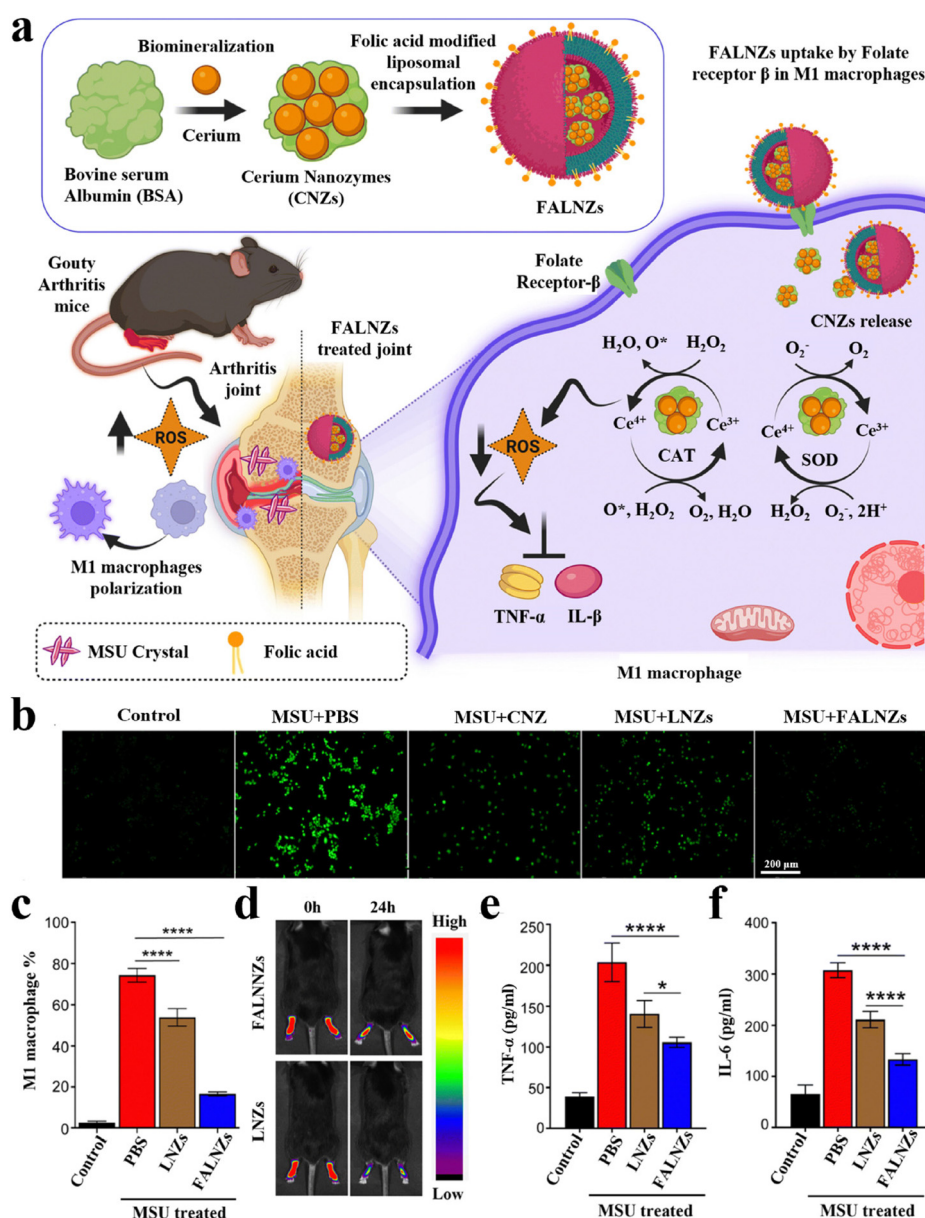


**Fig. 4** Biomineralized metallic nanozymes for anti-inflammatory therapy. (a) Fabrication of FALNZs and its therapeutic mechanism in gouty arthritis model. (b) Intracellular ROS levels were detected using the DCFH-DA probe. Scale bar: 200 μm. (c) The M1 macrophage numbers after treatment with MSU and FALNZs. (d) *In vivo* FI of the mice after injection of IR780-labeled FALNZs and IR780-labeled LNZs, respectively. (e) The serum TNF-α and (f) IL-6 levels measured by ELISA. Modified from ref. 130 with permission. Copyright 2023 Royal Society of Chemistry.

mechanisms, the intestinal oxidative stress induced by excess reactive oxygen species (ROS) is thought to play a key role in the pathogenesis and progression of IBD.<sup>122–124</sup> Therefore, removing ROS from the intestine may be beneficial to alleviate the symptoms of IBD. Superoxide dismutase (SOD), is an anti-oxidant enzyme that can convert superoxide radicals into oxygen and hydrogen peroxide, reducing the damage of toxic radicals to the body and thus has great potential in alleviating IBD.<sup>125</sup> However, under the harsh conditions of the gastrointestinal tract, direct oral administration of SOD may lead to issues such as premature release, disintegration, and rapid clearance. The use of biocompatible nanodrug delivery systems may overcome the deficiency of direct oral delivery and be beneficial to improve the solubility, permeability, and gastrointestinal stability of SOD. Bai *et al.* constructed a biocompatible nanocomposite (SOD@ZIF-zni) by encapsulating SOD in ZIF-zni using a biomimetic mineralization method for the treatment of IBD.<sup>126</sup> Owing to the protection of the ZIF-zni layer, the stability and catalytic activity of SOD@ZIF-zni were significantly improved compared with SOD in the simulated gastrointestinal environment, especially in the acidic pH conditions of the stomach. In the dextran sulfate sodium-induced colitis mice model, oral administration of SOD@ZIF-zni effectively eliminated the superoxide anions, inhibiting the secretion of pro-inflammatory cytokines (IL-1 $\beta$ , IL-6, and TNF- $\alpha$ ) in the inflamed colon tissue, resulting in the alleviation of colitis. Together, this study provided an effective strategy for constructing the delivery system of enzymes and expanded the application of biomimetic mineralized nanoplateforms in oral drug delivery, providing a valuable strategy for the treatment of other gastrointestinal diseases.

Gouty arthritis is the most common inflammatory arthritis worldwide, mainly caused by the accumulation of monosodium urate (MSU) crystals in the joint.<sup>127</sup> The main symptoms include redness, swelling, pain, or limited mobility in the limb joints within a few hours. The accumulation of MSU crystals can activate the secretion of a series of pro-inflammatory cytokines and the production of excessive ROS, leading to exacerbation of inflammation and even bone erosion.<sup>128,129</sup> The activated inflammatory M1 macrophages plays a key role in this process. Therefore, inhibiting the activation of M1 macrophage and alleviating oxidative stress at the inflammatory site are beneficial for the treatment of gouty arthritis. Various anti-inflammatory drugs and small molecule drugs have been reported to be delivered to joints *via* nanocarriers to reduce the inflammatory response. However, the therapeutic efficacy of these nanomedicines is not ideal due to the lack of targeting and susceptibility to rapid clearance. In virtue of the high affinity between folic acid (FA) and folate receptor, Park *et al.* designed a biom mineralized NPs (named FALNZs) that actively targeted M1 macrophages to treat gouty arthritis (Fig. 4a).<sup>130</sup> FALNZs were composed of BSA-biom mineralized cerium oxide nanozymes (CNZs, as a core) and FA-modified liposomes (as a shell). The cellular uptake results showed that the uptake of FALNZs by M1 macrophages was significantly enhanced compared with the NPs without FA modification (LNZs group). Due to the enzyme-like activities of CNZs (SOD-

like and CAT-like),<sup>131</sup> FALNZs exhibited an excellent ROS scavenging capability at the inflammatory sites (Fig. 4b). In addition, FALNZs showed a strong macrophage polarization capability, greatly reducing the proportion of M1 macrophages (Fig. 4c). In a mouse model of MSU-induced gouty arthritis, the intra-articular injection of FALNZs could effectively target inflammatory macrophages (Fig. 4d). In addition, FALNZs could effectively relieve joint swelling, inhibiting the production of pro-inflammatory cytokines (Fig. 4e and f), and alleviating the pathological characteristics of the joint site.

## 4. Conclusion and perspectives

Due to their characteristics of simple preparation and excellent biocompatibility, as well as biodegradability, PMNMs have received enormous attention. In this review, we initially summarized the general construction principles and strategies for constructing PMNMs (including *in situ* mineralization strategy and genetic engineering strategy). More importantly, we summarized the development of PMNMs in biomedical applications, including bioimaging (MRI, FI, and bimodal imaging), as well as anti-tumor, anti-bacterial, and anti-inflammatory therapies. Firstly, in terms of bioimaging, imaging probes with targeting and specificity can be easily fabricated *via* rational design and protein-directed biomineralization and biomimetic mineralization techniques. These nanomaterials tend to have lower *in vivo* toxicity and better biodegradability, compared to those probes composed of pure inorganic nanomaterials. In addition, nanoprobe with microenvironment responsiveness can also be designed on the basis of the pathological characteristics of lesions. Compared to non-lesion tissues, the imaging contrast of these probes at the lesion could be greatly enhanced, which could be conducive to improving the accuracy and credibility of early diagnosis of diseases. Secondly, in the field of anti-tumor therapy, biocompatible and biodegradable nanomaterials can be prepared through protein-directed biomineralization and biomimetic mineralization techniques. These nanomaterials can serve as crucial carriers for therapeutic drugs, delivering small molecule drugs or therapeutic proteins (such as GOx) to the tumor site in a targeted way and releasing them, thereby improving the therapeutic efficacy. These smart nanomaterials can also be used for PTT, PDT, and CDT. These new modalities of cancer treatment will contribute to complete tumor eradication. Thirdly, in terms of anti-bacterial application, these prepared nanomaterials have excellent anti-bacterial properties, strong biofilm destruction ability, and the superior ability to promote wound healing, making them very promising in the treatment of drug-resistant bacterial infections. Finally, in terms of anti-inflammatory therapy, organic-inorganic nanomaterials prepared by protein-mediated biomineralization and biomimetic mineralization technology offered superior activities of anti-oxidant enzymes, which could effectively scavenge ROS at the inflammatory sites and inhibit the production of pro-inflammatory cytokines, helping to alleviate the symptoms of inflammatory disease.

Although significant progress has been made in the application research of disease treatment by the nanomaterials fabricated through biomineralization technique, there are still some key issues that remain to be addressed, to meet the needs of practical clinical applications. Firstly, it is crucial to optimize the preparation process to obtain biomineralized nanomaterials with uniform structures and stable properties. Secondly, further design and modification of nanomaterials to achieve more precise organ-targeting to improve bioavailability and therapeutic efficacy. Thirdly, the toxic side effects of the modified nanomaterials should be reduced to meet the standards for clinical application. Finally, it is necessary to elucidate the conditions under which nanomaterials function *in vivo* and the mechanisms of degradation *in vivo*. With the continuous innovation of nanotechnology and the further deepening of follow-up research, PMNMs will eventually overcome various difficulties in clinical practice and realize the unity of disease diagnosis and treatment.

## Author contributions

Da-Gui Zhang: conceptualization, writing – original draft; Yu-Jing Pan: conceptualization, writing – original draft; Biao-Qi Chen: conceptualization, supervision, writing – review & editing; Xiao-Chang Lu: writing – review & editing; Qin-Xi Xu: writing – review & editing; Pei Wang: writing – review & editing, funding acquisition; Ranjith Kumar Kankala: writing – review & editing; Ni-Na Jiang: writing – review & editing; Shi-Bin Wang: writing – review & editing, funding acquisition; Ai-Zheng Chen: supervision, funding acquisition, writing – review & editing.

## Conflicts of interest

There are no conflicts of interest to declare.

## Acknowledgements

The financial support from the National Natural Science Foundation of China (NSFC, 81971734, 32071323, and 32271410), the Science and Technology Projects in Fujian Province (2022FX1, 2023Y4008), the Jiangxi Provincial Natural Science Foundation (20224BAB216078, 20232BAB206135), and the Program for Innovative Research Team in Science and Technology in Fujian Province University.

## References

- 1 G. Mirabello, J. J. M. Lenders and N. A. J. M. Sommerdijk, *Chem. Soc. Rev.*, 2016, **45**, 5085–5106.
- 2 S. Yao, B. Jin, Z. Liu, C. Shao, R. Zhao, X. Wang and R. Tang, *Adv. Mater.*, 2017, **29**, 1605903.
- 3 A. George and A. Veis, *Chem. Rev.*, 2008, **108**, 4670–4693.
- 4 L. Zhou, Z. Chen, K. Dong, M. Yin, J. Ren and X. Qu, *Biomaterials*, 2014, **35**, 8694–8702.
- 5 Y. Ding, M. Cai, P. Niu, H. Zhang, S. Zhang and Y. Sun, *Composites, Part B*, 2022, **244**, 110196.
- 6 A. Veis, *Science*, 2005, **307**, 1419–1420.
- 7 I. M. Weiss, N. Tuross, L. Addadi and S. Weiner, *J. Exp. Zool.*, 2002, **293**, 478–491.
- 8 Y. Zhao and R. Tang, *Acta Biomater.*, 2021, **120**, 57–80.
- 9 Z. Nie, Y. Zhang, R. Tang and X. Wang, *J. Inorg. Biochem.*, 2022, **232**, 111815.
- 10 A. S. Deshpande and E. Beniash, *Cryst. Growth Des.*, 2008, **8**, 3084–3090.
- 11 J. D. Hartgerink, E. Beniash and S. I. Stupp, *Science*, 2001, **294**, 1684–1688.
- 12 L. Mao, H. Gao, H. Yao, L. Liu, H. Colfen, G. Liu, S. Chen, S. Li, Y. Yan, Y. Liu and S. Yu, *Science*, 2016, **354**, 107–110.
- 13 Q. Ruan, N. Siddiqah, X. Li, S. Nutt and J. Moradian-Oldak, *Connect. Tissue Res.*, 2014, **55**, 150–154.
- 14 N. Tang, H. Li, L. Zhang, X. Zhang, Y. Chen, H. Shou, S. Feng, X. Chen, Y. Luo, R. Tang and B. Wang, *Angew. Chem., Int. Ed.*, 2021, **60**, 6509–6517.
- 15 L. Dong, J. Ding, L. Zhu, Y. Liu, X. Gao and W. Zhou, *Chin. Chem. Lett.*, 2023, **34**, 108192.
- 16 Y. Wang, C. X. Yang and X. P. Yan, *Nanoscale*, 2017, **9**, 9049–9055.
- 17 P. Wang, M. Xiao, H. Pei, H. Xing, S. Luo, C. Tsung and L. Li, *Chem. Eng. J.*, 2021, **415**, 129036.
- 18 Y. Pan, Y. Zhang, B. Chen, Y. Zhao, J. Wang, C. Li, D. Zhang, R. K. Kankala, S. Wang, G. Liu and A. Chen, *Bioact. Mater.*, 2024, **33**, 311–323.
- 19 Y. Liu, B. Yu, X. Dai, N. Zhao and F. Xu, *Biomaterials*, 2021, **274**, 120885.
- 20 G. Wang, X. Li, L. Mo, Z. Song, W. Chen, Y. Deng, H. Zhao, E. Qin, C. Qin and R. Tang, *Angew. Chem., Int. Ed.*, 2012, **51**, 10576–10579.
- 21 H. Liang, F. Sheng, B. Zhou, Y. Pei, B. Li and J. Li, *Int. J. Biol. Macromol.*, 2017, **102**, 218–224.
- 22 C. Ruiz-Agudo, J. Lutz, P. Keckeis, M. King, A. Marx and D. Gebauer, *J. Am. Chem. Soc.*, 2019, **141**, 12240–12245.
- 23 J. Zhang, Y. Ji, S. Jiang, M. Shi, W. Cai, R. J. Miron and Y. Zhang, *Adv. Sci.*, 2021, **8**, 2100363.
- 24 V. Uskokovic and D. P. Uskokovic, *J. Biomed. Mater. Res., Part B*, 2011, **96B**, 152–191.
- 25 C. Qi, J. Lin, L. H. Fu and P. Huang, *Chem. Soc. Rev.*, 2018, **47**, 357–403.
- 26 C. C. Cenker, P. H. H. Bomans, H. Friedrich, B. Dedeoglu, V. Aviyente, U. Olsson, N. A. J. M. Sommerdijk and S. Bucak, *Soft Matter*, 2012, **8**, 7463–7470.
- 27 W. Wang, X. Liu, X. Zheng, H. J. Jin and X. Li, *Adv. Healthcare Mater.*, 2020, **9**, 2001117.
- 28 D. Gebauer, M. Kellermeier, J. D. Gale, L. Bergstrom and H. Coelfen, *Chem. Soc. Rev.*, 2014, **43**, 2348–2371.
- 29 J. J. De Yoreo, P. U. P. A. Gilbert, N. A. J. M. Sommerdijk, R. L. Penn, S. Whitelam, D. Joester, H. Zhang, J. D. Rimer, A. Navrotsky, J. F. Banfield, A. F. Wallace, F. M. Michel,

- F. C. Meldrum, H. Coelfen and P. M. Dove, *Science*, 2015, **349**, aaa6760.
- 30 D. Gebauer and H. Coelfen, *Nano Today*, 2011, **6**, 564–584.
- 31 X. Wang, J. Yang, C. M. Andrei, L. Soleymani and K. Grandfield, *Commun. Chem.*, 2018, **1**, 80.
- 32 Q. Yu, Y. Tian, M. Li, Y. Jiang, H. Sun, G. Zhang, Z. Gao, W. Zhang, J. Hao, M. Hu and J. Cui, *Chem. Commun.*, 2020, **56**, 11078–11081.
- 33 S. Weiner, Y. Levi-Kalisman, S. Raz and L. Addadi, *Connect. Tissue Res.*, 2003, **44**, 214–218.
- 34 R. Dillaman, S. Hequembourg and M. Gay, *J. Morphol.*, 2005, **263**, 356–374.
- 35 C. E. Killian, R. A. Metzler, Y. U. T. Gong, I. C. Olson, J. Aizenberg, Y. Politi, F. H. Wilt, A. Scholl, A. Young, A. Doran, M. Kunz, N. Tamura, S. N. Coppersmith and P. U. P. A. Gilbert, *J. Am. Chem. Soc.*, 2009, **131**, 18404–18409.
- 36 J. Mahamid, A. Sharir, L. Addadi and S. Weiner, *Proc. Natl. Acad. Sci. U. S. A.*, 2008, **105**, 12748–12753.
- 37 T. Titma, *Toxicol. In Vitro*, 2018, **50**, 11–21.
- 38 N. Lee, D. A. Sverjensky and R. M. Hazen, *Environ. Sci. Technol.*, 2014, **48**, 9358–9365.
- 39 M. Li, Y. Wang, T. Li, J. Zhang, X. Wang, J. Luo, M. You, T. Yang, Y. Deng, H. Yang and H. Ke, *Acta Biomater.*, 2023, **155**, 564–574.
- 40 L. Han, H. Zhang, D. Chen and F. Li, *Adv. Funct. Mater.*, 2018, **28**, 1800018.
- 41 L. Fu, C. Qi, T. Sun, K. Huang, J. Lin and P. Huang, *Exploration*, 2023, 20210110.
- 42 L. Fu, Y. Wan, C. Li, C. Qi, T. He, C. Yang, Y. Zhang, J. Lin and P. Huang, *Adv. Funct. Mater.*, 2021, **31**, 2009848.
- 43 N. Wang, G. Zhang, P. Zhang, K. Zhao, Y. Tian and J. Cui, *Adv. Healthcare Mater.*, 2023, **12**, 2300249.
- 44 T. T. Chen, J. T. Yi, Y. Y. Zhao and X. Chu, *J. Am. Chem. Soc.*, 2018, **140**, 9912–9920.
- 45 D. I. Pattison, A. S. Rahmanto and M. J. Davies, *Photochem. Photobiol. Sci.*, 2012, **11**, 38–53.
- 46 J. Pan, Y. Wang, H. Pan, C. Zhang, X. Zhang, Y. Fu, X. Zhang, C. Yu, S. Sun and X. Yan, *Adv. Funct. Mater.*, 2017, **27**, 1603440.
- 47 B. Xiao, X. Zhou, H. Xu, B. Wu, D. Hu, H. Hu, K. Pu, Z. Zhou, X. Liu, J. Tang and Y. Shen, *ACS Nano*, 2018, **12**, 12682–12691.
- 48 Z. Wang, P. Huang, O. Jacobson, Z. Wang, Y. Liu, L. Lin, J. Lin, N. Lu, H. Zhang, R. Tian, G. Niu, G. Liu and X. Chen, *ACS Nano*, 2016, **10**, 3453–3460.
- 49 P. M. Harrison and P. Arosio, *Biochim. Biophys. Acta*, 1996, **1275**, 161–203.
- 50 P. Huang, P. Rong, A. Jin, X. Yan, M. G. Zhang, J. Lin, H. Hu, Z. Wang, X. Yue, W. Li, G. Niu, W. Zeng, W. Wang, K. Zhou and X. Chen, *Adv. Mater.*, 2014, **26**, 6401–6408.
- 51 R. Fan, S. W. Chew, V. V. Cheong and B. P. Orner, *Small*, 2010, **6**, 1483–1487.
- 52 Q. Liu, J. Tian, J. Liu, M. Zhu, Z. Gao, X. Hu, A. C. Midgley, J. Wu, X. Wang, D. Kong, J. Zhuang, J. Liu, X. Yan and X. Huang, *Adv. Mater.*, 2021, **33**, 2103128.
- 53 B. Jiang, L. Yan, J. L. Zhang, M. Zhou, G. Z. Shi, X. Y. Tian, K. L. Fan, C. Y. Hao and X. Y. Yan, *ACS Appl. Mater. Interfaces*, 2019, **11**, 9747–9755.
- 54 H. Veroniaina, Z. Wu and X. Qi, *J. Adv. Res.*, 2021, **33**, 201–213.
- 55 M. Uchida, M. L. Flenniken, M. Allen, D. A. Willits, B. E. Crowley, S. Brumfield, A. F. Willis, L. Jackiw, M. Jutila, M. J. Young and T. Douglas, *J. Am. Chem. Soc.*, 2006, **128**, 16626–16633.
- 56 B. Jiang, L. Yan, J. Zhang, M. Zhou, G. Shi, X. Tian, K. Fan, C. Hao and X. Yan, *ACS Appl. Mater. Interfaces*, 2019, **11**, 9747–9755.
- 57 E. Fantechi, C. Innocenti, M. Zanardelli, M. Fittipaldi, E. Falvo, M. Carbo, V. Shullani, L. D. C. Mannelli, C. Ghelardini, A. M. Ferretti, A. Ponti, C. Sangregorio and P. Ceci, *ACS Nano*, 2014, **8**, 4705–4719.
- 58 Z. T. Wang, H. Y. Gao, Y. Zhang, G. Liu, G. Niu and X. Y. Chen, *Front. Chem. Sci. Eng.*, 2017, **11**, 633–646.
- 59 K. Zeth, E. Hoiczky and M. Okuda, *Trends Biochem. Sci.*, 2016, **41**, 190–203.
- 60 B. Bhushan, S. U. Kumar, I. Matai, A. Sachdev, P. Dubey and P. Gopinath, *J. Biomed. Nanotechnol.*, 2014, **10**, 2950–2976.
- 61 Y. Zhang, X. Wang, C. Chu, Z. Zhou, B. Chen, X. Pang, G. Lin, H. Lin, Y. Guo, E. Ren, P. Lv, Y. Shi, Q. Zheng, X. Yan, X. Chen and G. Liu, *Nat. Commun.*, 2020, **11**, 5421.
- 62 M. Wang, L. Zhang, Y. Cai, Y. Yang, L. Qu, Y. Shen, J. Jin, J. Zhou and J. Chen, *ACS Nano*, 2020, **14**, 17405–17418.
- 63 Y. Shen, M. Wang, H. Wang, J. Zhou and J. Chen, *ACS Appl. Mater. Interfaces*, 2022, **14**, 19907–19917.
- 64 L. Fass, *Mol. Oncol.*, 2008, **2**, 115–152.
- 65 C. Wang, Q. Liu, X. Huang and J. Zhuang, *J. Mater. Chem. B*, 2023, **11**, 4153–4170.
- 66 D. Pan, S. D. Caruthers, J. Chen, P. M. Winter, A. SenPan, A. H. Schmieder, S. A. Wickline and G. M. Lanza, *Future Med. Chem.*, 2010, **2**, 471–490.
- 67 L. Zhang, Q. Chen, X. Zou, J. Chen, L. Hu, Z. Dong, J. Zhou, Y. Chen, Z. Liu and L. Cheng, *J. Mater. Chem. B*, 2019, **7**, 5170–5181.
- 68 L. Dong, X. Zhang, L. Cai, F. Zuo, M. Zhao, Q. Wang, S. Zhang, K. Xu and J. Li, *Biomed. Pharmacother.*, 2020, **130**, 110585.
- 69 R. Song, M. Ruan, J. Dai and W. Xue, *J. Mater. Chem. B*, 2021, **9**, 2494–2504.
- 70 Y. Wang, C. Xu, Y. Chang, L. Zhao, K. Zhang, Y. Zhao, F. Gao and X. Gao, *ACS Appl. Mater. Interfaces*, 2017, **9**, 28959–28966.
- 71 C. Pereira, A. M. Pereira, M. Rocha, C. Freire and C. F. G. C. Geraldés, *J. Mater. Chem. B*, 2015, **3**, 6261–6273.
- 72 F. Wang, L. Wen, J. Liu, W. Peng, Z. Meng, Q. Chen, Y. Wang, B. Ke, Y. Guo and P. Mi, *Biomaterials*, 2020, **230**, 119614.
- 73 X. Shu, A. Royant, M. Z. Lin, T. A. Aguilera, V. Lev-Ram, P. A. Steinbach and R. Y. Tsien, *Science*, 2009, **324**, 804–807.

- 74 M. L. Liu, B. B. Chen, C. M. Li and C. Z. Huang, *Green Chem.*, 2019, **21**, 449–471.
- 75 K. Welsher, Z. Liu, S. P. Sherlock, J. T. Robinson, Z. Chen, D. Daranciang and H. Dai, *Nat. Nanotechnol.*, 2009, **4**, 773–780.
- 76 J. Zhang, G. Hao, C. Yao, J. Yu, J. Wang, W. Yang, C. Hu and B. Zhang, *ACS Appl. Mater. Interfaces*, 2016, **8**, 16612–16621.
- 77 D. Cui, L. Han, W. Jiang, L. Chen and N. Niu, *ACS Appl. Nano Mater.*, 2023, **6**, 1303–1314.
- 78 Y. Cheng, Y. Zhao, H. Yuan, H. Zhou, J. Xu, X. Chen, K. Zhang, R. Antoine and S. Zhang, *Sens. Actuators, B*, 2023, **394**, 134427.
- 79 J. Zhang, M. Sajid, N. Na, L. Huang, D. He and J. Ouyang, *Biosens. Bioelectron.*, 2012, **35**, 313–318.
- 80 C. Sun, H. Yang, Y. Yuan, X. Tian, L. Wang, Y. Guo, L. Xu, J. Lei, N. Gao, G. J. Anderson, X.-J. Liang, C. Chen, Y. Zhao and G. Nie, *J. Am. Chem. Soc.*, 2011, **133**, 8617–8624.
- 81 Y. Li, Y. Cao, L. Wei, J. Wang, M. Zhang, X. Yang, W. Wang and G. Yang, *Acta Biomater.*, 2020, **101**, 436–443.
- 82 J. Sun, H. Wu and Y. Jin, *Nanoscale*, 2014, **6**, 5449–5457.
- 83 N. Zhang, Y. Si, Z. Sun, L. Chen, R. Li, Y. Qiao and H. Wang, *Anal. Chem.*, 2014, **86**, 11714–11721.
- 84 D. Cheng, W. Xu, X. Gong, L. Yuan and X. B. Zhang, *Acc. Chem. Res.*, 2021, **54**, 403–415.
- 85 C. Wang, Z. Wang, T. Zhao, Y. Li, G. Huang, B. D. Sumer and J. Gao, *Biomaterials*, 2018, **157**, 62–75.
- 86 X. Han, K. Xu, O. Taratula and K. Farsad, *Nanoscale*, 2019, **11**, 799–819.
- 87 M. Luo, H. Yukawa, K. Sato, M. Tozawa, M. Tokunaga, T. Kameyama, T. Torimoto and Y. Baba, *ACS Appl. Mater. Interfaces*, 2022, **14**, 34365–34376.
- 88 A. Jemal, F. Bray, M. M. Center, J. Ferlay, E. Ward and D. Forman, *Ca-Cancer J. Clin.*, 2011, **61**, 69–90.
- 89 Z. Chen, R. K. Kankala, Z. Yang, W. Li, S. Xie, H. Li, A. Chen and L. Zou, *Theranostics*, 2022, **12**, 3719–3746.
- 90 C. L. Chaffer and R. A. Weinberg, *Science*, 2011, **331**, 1559–1564.
- 91 J. Couzin, *Science*, 2008, **321**, 1146–1147.
- 92 A. D. Levinson, *Science*, 2010, **328**, 137–137.
- 93 L. Fu, Y. Zhang, R. A. Farokhzad, B. B. Mendes, J. Conde and J. Shi, *Chem. Soc. Rev.*, 2023, **52**, 7579–7601.
- 94 L. Fu, C. Li, W. Yin, Y. Hu, T. Sun, Y. Wan, J. Lin, Z. Li and P. Huang, *Adv. Healthcare Mater.*, 2021, **10**, 2101563.
- 95 B. Chen, Y. Zhao, Y. Zhang, Y. Pan, H. Xia, R. K. Kankala, S. Wang, G. Liu and A. Chen, *Bioact. Mater.*, 2023, **21**, 1–19.
- 96 B. Chen, W. Dai, B. He, H. Zhang, X. Wang, Y. Wang and Q. Zhang, *Theranostics*, 2017, **7**, 538–558.
- 97 X. Li, Z. Huang, Z. Liao, A. Liu and S. Huo, *Nanoscale*, 2023, **15**, 8532–8547.
- 98 Z. Fang, S. Pan, P. Gao, H. Sheng, L. Li, L. Shi, Y. Zhang and X. Cai, *Int. J. Pharm.*, 2020, **575**, 118841.
- 99 Z. Xie, Q. Jia, S. Wu, L. Hao, J. Liu, C. Guo, H. Tian, C. Li and Z. Li, *J. Drug Delivery Sci. Technol.*, 2023, **88**, 104960.
- 100 W. Fan, B. Yung, P. Huang and X. Chen, *Chem. Rev.*, 2017, **117**, 13566–13638.
- 101 D. Zhang, B. Chen, Y. Pan, H. Liu, Y. Shi, L. Chen, R. K. Kankala, S. Wang and A. Chen, *Mater. Des.*, 2023, **227**, 111794.
- 102 R. Yang, M. Hou, Y. Gao, S. Lu, L. Zhang, Z. Xu, C. M. Li, Y. Kang and P. Xue, *Theranostics*, 2019, **9**, 6314–6333.
- 103 C. Li, Y. Wan, Y. Zhang, L. Fu, N. T. Blum, R. Cui, B. Wu, R. Zheng, J. Lin, Z. Li and P. Huang, *Adv. Mater.*, 2022, **34**, 2103980.
- 104 C. Zhang, W. Bu, D. Ni, S. Zhang, Q. Li, Z. Yao, J. Zhang, H. Yao, Z. Wang and J. Shi, *Angew. Chem., Int. Ed.*, 2016, **55**, 2101–2106.
- 105 L. H. Fu, Y. Wan, C. Qi, J. He, C. Li, C. Yang, H. Xu, J. Lin and P. Huang, *Adv. Mater.*, 2021, **33**, 2006892.
- 106 S. Lakhundi and K. Zhang, *Clin. Microbiol. Rev.*, 2018, **31**, 20–122.
- 107 H. Chen, Y. Jin, J. Wang, Y. Wang, W. Jiang, H. Dai, S. Pang, L. Lei, J. Ji and B. Wang, *Nanoscale*, 2018, **10**, 20946–20962.
- 108 P. Gupta, S. Sarkar, B. Das, S. Bhattacharjee and P. Tribedi, *Arch. Microbiol.*, 2016, **198**, 1–15.
- 109 J. M. V. Makabenta, A. Nabawy, C. H. Li, S. Schmidt-Malan, R. Patel and V. M. Rotello, *Nat. Rev. Microbiol.*, 2021, **19**, 23–36.
- 110 X. Fei, M. Jia, X. Du, Y. Yang, R. Zhang, Z. Shao, X. Zhao and X. Chen, *Biomacromolecules*, 2013, **14**, 4483–4488.
- 111 J. Li, Q. Li, X. Ma, B. Tian, T. Li, J. Yu, S. Dai, Y. Weng and Y. Hua, *Int. J. Nanomed.*, 2016, **11**, 5931–5944.
- 112 S. Zhao, Y. Gao, J. Tan, Y. Zhu, X. Ying, M. Zhang, X. Yu and B. You, *SN Appl. Sci.*, 2019, **1**, 917.
- 113 M. Ghaffarlou, S. Ilk, H. Rahimi, H. Danafar, M. Barsbay and A. Sharafi, *Nanomedicine*, 2022, **17**, 2145–2155.
- 114 J. Huang, J. Zhou, J. Zhuang, H. Gao, D. Huang, L. Wang, W. Wu, Q. Li, D. P. Yang and M. Y. Han, *ACS Appl. Mater. Interfaces*, 2017, **9**, 36606–36614.
- 115 Y. Zhang, L. Lai, Y. Liu, B. Chen, J. Yao, P. Zheng, Q. Pan and W. Zhu, *ACS Appl. Mater. Interfaces*, 2022, **14**, 6453–6464.
- 116 F. Cao, S. Gui, X. Gao, W. Zhang, Z. Fu, L. Tao, Z. Jiang, X. Chen, H. Qian and X. Wang, *Mater. Des.*, 2022, **218**, 110686.
- 117 A. S. Bagad, J. A. Joseph, N. Bhaskaran and A. Agarwal, *Adv. Pharmacol. Sci.*, 2013, **2013**, 805756–805756.
- 118 S. Reuter, S. C. Gupta, M. M. Chaturvedi and B. B. Aggarwal, *Free Radicals Biol. Med.*, 2010, **49**, 1603–1616.
- 119 Y. Tang, X. Zhou, T. Cao, E. Chen, Y. Li, W. Lei, Y. Hu, B. He and S. Liu, *DNA Cell Biol.*, 2022, **41**, 924–934.
- 120 M. Ghasemian, S. Owlia and M. B. Owlia, *Adv. Pharmacol. Sci.*, 2016, **2016**, 9130979–9130979.
- 121 Y. Z. Zhang and Y. Y. Li, *World J. Gastroenterol.*, 2014, **20**, 91–99.
- 122 Y. Wang, L. Li, W. Zhao, Y. Dou, H. An, H. Tao, X. Xu, Y. Jia, S. Lu, J. Zhang and H. Hu, *ACS Nano*, 2018, **12**, 8943–8960.



- 123 A. Larabi, N. Barnich and H. T. T. Nguyen, *Autophagy*, 2020, **16**, 38–51.
- 124 J. Zhao, W. Gao, X. Cai, J. Xu, D. Zou, Z. Li, B. Hu and Y. Zheng, *Theranostics*, 2019, **9**, 2843–2855.
- 125 Y. Sheng, H. Li, M. Liu, B. Xie, W. Wei, J. Wu, F. Meng, H. Y. Wang and S. Chen, *Inflamm. Bowel Dis.*, 2019, **25**, 1644–1655.
- 126 S. Bai, X. Shao, Y. Tao, S. Wang, H. Han and Q. Li, *J. Mater. Chem. B*, 2022, **10**, 5174–5181.
- 127 L. Wilson and J. J. Saseen, *Pharmacotherapy*, 2016, **36**, 906–922.
- 128 J. M. Bennett, G. Reeves, G. E. Billman and J. P. Sturmberg, *Front. Biomed.*, 2018, **5**, 316.
- 129 X. Ouyang, N. Li, M. Guo, M. Zhang, J. Cheng, L. Yi and J. Zhu, *Front. Pharmacol.*, 2021, **12**, 760331.
- 130 A. Mohapatra, A. Mohanty, P. Sathiyamoorthy, S. Chahal, V. Vijayan, S. K. Rajendrakumar and I. K. Park, *J. Mater. Chem. B*, 2023, **11**, 7684–7695.
- 131 S. Dong, Y. Dong, B. Liu, J. Liu, S. Liu, Z. Zhao, W. Li, B. Tian, R. Zhao, F. He, S. Gai, Y. Xie, P. Yang and Y. Zhao, *Adv. Mater.*, 2022, **34**, 2107054.